STUDIA UBB CHEMIA, LXIX, 1, 2024 (p. 51-68)
(RECOMMENDED CITATION)
DOI:10.24193/subbchem.2024.1.04

EFFECT OF THALLIUM (I) IONS ON THE ZINC ELECTROWINNING PROCESS

Ning YUAN[a], Xi CHEN[a], Xing LIU[a], Lin FU[a], Yan CUI[a,*], Shihong HUANG[b,*], Wenjia ZHAO[a]

ABSTRACT. The effects of thallium(Ⅰ) ions on the surface morphology, cathode current efficiency, cathode potential, polarization behavior, and electrochemical impedance spectroscopy of zinc electrowinning were studied by scanning electron microscopy and electrochemical measurements. The results showed that with increasing thallium(Ⅰ) ion concentration in the electrolyte, the hydrogen evolution reaction and the galvanic effect produced during zinc electrowinning increased. When the concentration of thallium(Ⅰ) ions in the electrolyte was 0.6 mg L^{-1}, the exchange current density of the zinc electrowinning process was maximum and the polarization was minimum. At this time, the R_{ct} of the equivalent circuit was minimum, the CPE value was minimum, and the charge transfer rate was maximum. The cathodic current efficiency decreased from 80% to 55% when the thallium(Ⅰ) ion concentration was 1.5 mg L^{-1}. The presence of thallium(Ⅰ) ions also affected the surface macro- and microstructure of the zinc deposits. This result confirmed that thallium(Ⅰ) ions have a significant negative influence on the electrowinning of zinc.

Keywords: *Zinc electrowinning; Thallium(Ⅰ) ions; Cathodic current efficiency; Cathodic polarization; Electrochemical impedance spectroscopy*

[a] *Kunming University, School of Chemistry and Chemical Engineering, No. 2 Puxin Road, Kunming Economic and Technological Development Zone, 650214, Kunming, China*
[b] *Kunming University, Office of Science and Technology, No. 2 Puxin Road, Kunming Economic and Technological Development Zone, 650214, Kunming, China*
* *Corresponding author victory_me@outlook.com, 65865070@qq.com*

INTRODUCTION

Following iron, aluminum, and copper, zinc is regarded as the fourth most widely used metal [1]. More than 80% of the world's zinc is produced by the roasting–leaching–purification–electrowinning method [2-4]. Among the four steps, electrowinning is particularly critical because it directly determines the power consumption and quality of zinc production; energy consumed during this step accounts for about 60% of the total energy consumption of the zinc hydrometallurgy process [5]. The presence of metallic impurities in the zinc electrolyte is a common problem in electrowinning. Ivan [6] has reported that due to the presence of higher concentrations of metal impurities such as Sb and Ge, the current efficiency was reduced and complete redissolution of the deposited metal occurred. Muresan et al. [7] have studied the influence of metal impurities such as Cd, Fe and Cu in zinc electrowinning and showed that zinc deposition was prevented when Cd and Cu were present in solution because they coprecipitated on the cathode. In addition, there are some metal impurities present that promote the hydrogen evolution reaction during the zinc electrowinning process and decrease the current efficiency. Zhu et al. [8] have discovered that the concentration of co-deposited iridium in the deposited zinc layer increased with increasing Ir(IV) ion concentration in the electrolyte. The iridium deposited on the cathode acted as an active site for hydrogen evolution. Furthermore, some electronegativity impurities, such as alkali metals Na, Mg, Ca, etc., can make the surface of the deposited zinc dim and porous, which can also promote the hydrogen evolution reaction [9]. There are also variable-valence impurities that perform cyclic redox reactions at the anode and cathode, respectively, leading to a decrease in current efficiency, such as Mn, Fe, etc.

Zinc sulfide concentrate, as the main raw material for zinc refining, is commonly accompanied by a certain amount of thallium, with a normal content of 5–20 g/t. However, the content of thallium in some lead-zinc deposits was particularly high [10]. Liu et al. [11] showed that the Pb-Zn ore materials were relatively enriched with Tl (15.1–87.7 mg kg^{-1}), while even higher accumulation existed in the electrostatic dust (3280–4050 mg kg^{-1}) and acidic waste (13300 mg kg^{-1}). Karbowska et al. [12] investigated the translocation of thallium from zinc–lead ores from the Cracow–Silesia Upland due to ore flotation processing and natural processes and the element's mobility in these samples as determined by sequential extraction in accordance with a modified BCR procedure. Liu et al. [13] investigated the capacity for adsorption of thallium(Ⅰ) by a common sulfide mineral (zinc sulfide) in aerobic and anaerobic environments, which revealed three mechanisms for adsorption on the ZnS surface (surface complexation, electrostatic action and oxidation promotion).

In 2005, the electrolytic zinc plant of Huludao Nonferrous Metals Group Co., Ltd. purchased tens of thousands of tons of soot and zinc raw materials with high thallium content due to the shortage of mineral resources. The thallium content of this zinc-mixed raw material was as high as 0.015%, and the neutral leaching solution contained thallium greater than 0.01 g/L, which directly affected the electrical efficiency [14]. Therefore, it is important to study the effect of thallium(Ⅰ) ions on conventional zinc hydrometallurgy systems. The characteristics of the electrodeposition of thallium powder from sulphate baths containing a relatively low Tl ion content (0.005–0.020 mol L^{-1}) were examined. The cathodic polarization curves for thallium electrodeposition were greatly affected by the bath composition and the pH. The percentage cathodic current efficiency was relatively low and increased with increasing concentration of Tl ions in the bath to a maximum of 17% [15]. In earlier studies, Clavilier et al. [16] perfomed the underpotential deposition (UPD) of Tl^+ on Pt(111) electrode, arguing that there is an equilibrium in the adsorption-desorption process. More recently, Rodriguez et al. [17] have studied extensively either the UPD and irreversible adsorption of Tl on Pt(111) and vicinal surfaces. They were able to ascribe the processes Tl/Tl^+ oxidation and anion adsorption on the Tl-modified surface. Additionally, the results obtained with stepped surfaces indicate that some of the features are clearly associated to the presence of Pt(111) surface domains (terraces). Mirghasem Hosseini et al. [18] have studied the effect of Tl(Ⅰ) on the hard gold alloy electrodeposition of Au–Co from acid baths. They found that with addition of thallium in the hard gold electroplating bath an enhancement and inhibition of the gold deposition were observed at low and high cathodic potentials, respectively. Addition of trace quantities of Tl^+ to gold plating baths have been found to yield bright gold electrodeposits of suitable morphology, purity and hardness with depolarization effect. It is proposed that Tl^+ through its depolarization effect decreases the electrode inhibition brought by adsorbed cyanide species and increases deposition rate of gold. However, in zinc hydrometallurgy, the presence of thallium(Ⅰ) ions will reduce the current efficiency of zinc electrowinning.

During the roasting process of zinc concentrate, 70–84% of the thallium in the raw material evaporated into the soot; only 16–30% of the thallium remained in the roasted sand. However, due to the large proportion of roasted soot, the percentage of thallium content in the soot was relatively low, which generally did not meet the requirements of thallium purification, and most of the soot was still mixed with roasted sand as leaching material. In the leaching process, thallium mostly entered the acidic leaching solution with zinc calcine. During the purification stage, when impurities such as copper and cadmium were removed from the leaching solution, approximately 70% of the thallium in the leaching material entered the copper-cadmium slag for

enrichment. The small amount of thallium remaining in the leaching residue mostly entered the volatile soot during the volatilization kiln treatment [19]. The standard electrode potential of thallium ($E^{o}_{Tl^{+}/Tl}$ = -0.336 V) is more positive than that of zinc ($E^{o}_{Zn^{2+}/Zn}$ = -0.762 V), Therefore, thallium(Ⅰ) ions in the electrolyte will prefer to deposit on the cathode surface and probably lead to increased hydrogen evolution. What's more, in zinc electrowinning, the presence of thallium(Ⅰ) ions causes a galvanic effect on the zinc plate during electrolysis, resulting in the re-dissolution of zinc, which reduces the current efficiency. More seriously, thallium can induce other impurities to make the zinc electrowinning process produce "plate-burning" phenomena, which adversely affect the product yield and technoeconomic indexes, leading to continuous fluctuations in production that cannot be carried out normally. As a result, the selective removal of thallium from the electrolyte is critical for the stability of electrolytic production. The main methods for removing thallium from solutions are precipitation [20], sulfidation, adsorption [21], electroflocculation, and substitution. In the conventional zinc hydrometallurgy system, thallium is removed by the oxidation-precipitation method in the leaching stage. In this process, it is usually necessary to ensure that the thallium content of the zinc sulfate solution sent to the purification process is less than 1.0 mg/L. Existing Tl extraction methods consume excessive Zn and often result in incomplete removal. Xiong introduced an optimized technique that incorporates lead(Ⅱ) (Pb(Ⅱ)) to form a Pb-Tl compound during Zn cementation [22]. In the purification stage, thallium is removed by the substitution method. By adding lead-zinc powder, the content of thallium in the new solution can be theoretically controlled within 0.1 mg/L [14, 23]. However, few studies on this topic have been reported so far.

In this context, the purpose of this work was to study the influence of thallium(Ⅰ) ions on long term electrowinning of zinc from sulfate electrolytes by analyzing current efficiency, cathodic potential, cathodic polarization behavior, electrochemical impedance spectroscopy, and deposit morphology.

RESULTS AND DISCUSSION

Current efficiency

The effect of the presence of thallium(Ⅰ) ions on the current efficiency of zinc electrowinning is shown in Fig. 1. It can be seen that the current efficiency increased slightly between 0 and 0.6 mg L^{-1} thallium(Ⅰ) ions.

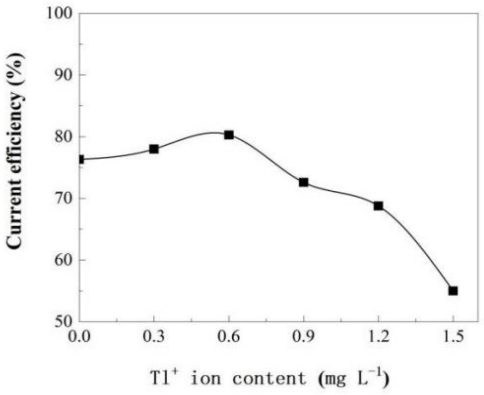

Figure 1. Effect of thallium(Ⅰ) ion content on the current efficiency of 24 h zinc deposition at a cathode current density of 518.86 A m^{-2}. Electrolyte: 35.46 g/L Zn^{2+} and 146.05 g/L H_2SO_4 electrolyte with varied Tl(Ⅰ) ions concentration (mg L^{-1}); temperature: 38 ± 1 ℃.

Since the standard electrode potential of thallium is more positive than that of zinc, thallium(Ⅰ) ions in the electrolyte will prefer to deposit on the cathode surface during zinc electrowinning. When thallium(Ⅰ) ions were present in the electrolyte, it probably led to increased hydrogen evolution, and the presence of thallium(Ⅰ) ions caused a galvanic effect on the zinc plate during electrolysis, resulting in the re-dissolution of the deposited zinc, which reduced the current efficiency [10]. The cathodic current efficiency decreased from 80% to 55% when 1.5 mg L^{-1} thallium(Ⅰ) ions were added to the electrolyte, as shown in Fig. 1. The above experiments confirmed that the presence of excess thallium(Ⅰ) ions in the electrolyte has a serious harmful effect on cathodic current efficiency. In actual production, considering that zinc electrowinning is a long-period continuous production method, if the content of thallium in the electrolyte was not controlled, thallium(Ⅰ) ions would gradually accumulate on the cathode surface via electrodeposition, thus probably increasing hydrogen evolution and causing a galvanic effect.

Deposit morphology

The concentration of thallium(Ⅰ) ions in the electrolyte was also found to greatly influence the morphology of the obtained zinc deposits. Deposited zinc was obtained by electrowinning in electrolytes with different thallium concentrations at a current density of 518.86 A m^{-2} for 24 h. The morphology of zinc deposition is shown in Figs. 2 and 3. Fig. 2 shows macroscopic photographs of the zinc plates, and Fig. 3 shows the corresponding SEM

micrographs. During the electrowinning process, a large number of circular holes were formed on the zinc plating surface regardless of the thallium(Ⅰ) ion concentration. However, there were significant differences in the size, roughness, and depth of the holes on different deposited zinc surfaces.

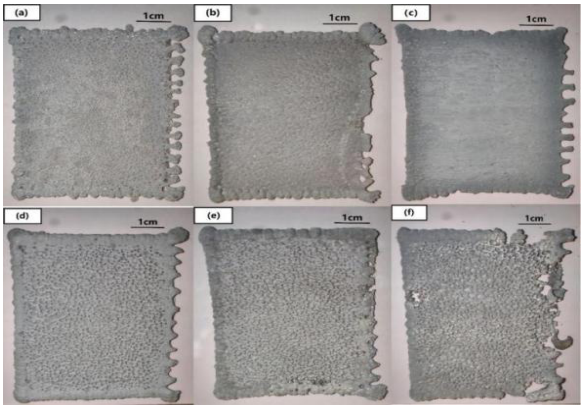

Figure 2. Photographs of zinc deposits showing the effect of various electrolyte thallium(Ⅰ) ion concentrations. (a) 0.0 mg L^{-1}, (b) 0.3 mg L^{-1}, (c) 0.6 mg L^{-1}, (d) 0.9 mg L^{-1}, (e) 1.2 mg L^{-1}, (f) 1.5 mg L^{-1}.

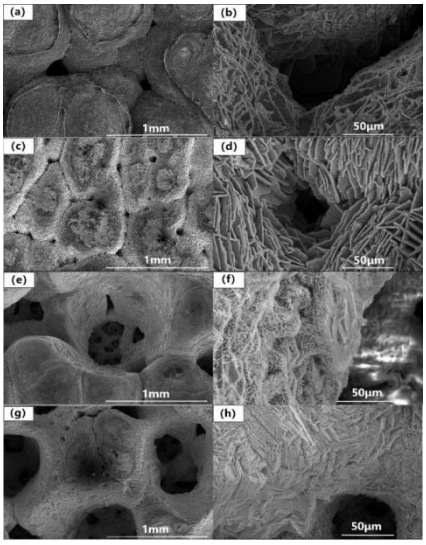

Figure 3. SEM micrographs showing the effect of electrolyte thallium(Ⅰ) ion concentrations on the morphology of deposits after electrowinning at 518.86 A m^{-2} for 24 h. (a) (b) 0.0 mg L^{-1}, (c) (d) 0.6 mg L^{-1}, (e) (f) 0.9 mg L^{-1}, (g) (h) 1.5 mg L^{-1} at different magnifications.

Zinc deposits obtained from impurity metal ion-free electrolytes usually consist of layers of flat platelets of dozens of micrometers in size. The SEM images of zinc deposited from the electrolyte containing 0.6 mg L^{-1} thallium(Ⅰ) ions showed that, similar to the zinc obtained from the impurity-free electrolyte, there were some obvious holes that may have caused gas evolution (Fig. 3(c) and (d)). When the thallium(Ⅰ) ion concentration increased from 0 mg L^{-1} to 0.6 mg L^{-1}, the surface of the deposited zinc was relatively flat, the holes were small, and the flaky deposition layers were stacked and relatively dense (Fig. 2(c) and Fig. 3(c), (d)). Further increase in the concentration of thallium(Ⅰ) ions in the electrolyte led to further changes in morphology. For example, when the thallium(Ⅰ) ion concentration increased from 0.6 mg L^{-1} to 1.5 mg L^{-1}, the surface of the deposited zinc was relatively rough and loose, and some deep holes appeared. These holes were large and embedded with small holes, and needle-like dendrites appeared on the flaky deposition layers (Fig. 2(f) and Fig. 3(g), (h)). It may be because the presence of thallium(Ⅰ) ions led to increased hydrogen evolution, resulting in the formation of a rough surface and some deep holes. Meanwhile, these morphologies could lead to further hydrogen evolution, during which small bubbles with a tendency to stick to the cathode surface could be formed. In addition, the deposited thallium and zinc formed microcells in the zinc electrowinning system. Where zinc, especially in the area connected to thallium, would redissolve and thallium would fall off from the cathode surface into the electrolyte. These led to the destruction of the cathode surface morphology.

Cathodic potential

The chronopotentiometric curves of the electrolytes with different thallium(Ⅰ) ion concentrations at 518.86 A m^{-2} cathode current density are shown in Fig. 4. The deposition potentials of zinc electrowinning under different thallium(Ⅰ) ion concentrations were obtained from Fig. 4. The effect of thallium(Ⅰ) ions on the cathodic potential of zinc electrowinning is shown in Fig. 5.

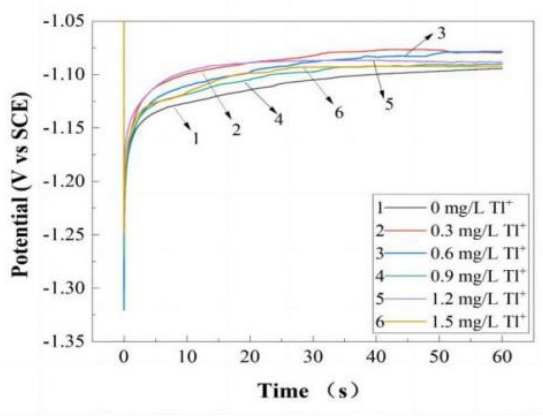

Figure 4. Chronopotentiometric curves measured in electrolytes with different thallium(Ⅰ) ion concentrations at 518.86 A m^{-2} cathode current density. Electrolyte: 35.46 g/L Zn^{2+} and 146.05 g/L H_2SO_4 electrolyte with varied Tl(Ⅰ) ions concentration (mg L^{-1}); temperature: 38 ± 1 ℃.

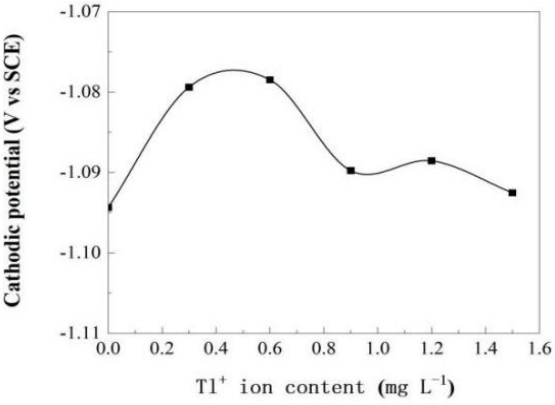

Figure 5. Effect of thallium(Ⅰ) ion concentration on cathodic potential curves for zinc deposition at a cathodic current density of 518.86 A m^{-2}. Electrolyte: 35.46 g/L Zn^{2+} and 146.05 g/L H_2SO_4 electrolyte with varied Tl(Ⅰ) ions concentration (mg L^{-1}); temperature: 38 ± 1 ℃.

As shown in Fig. 5, when the thallium(Ⅰ) ion concentration increased from 0 mg L^{-1} to 0.6 mg L^{-1}, the increase in cathode potential (becoming more positive) was caused by the increasing amount of current going to the hydrogen evolution reaction (HER) due to the depolarization of small amounts of thallium(Ⅰ) ions in zinc electrowinning. When the thallium(Ⅰ) ion concentration in the electrolyte increased from 0.6 mg L^{-1} to 1.5 mg L^{-1}, the

cathode potential decreased from -1.08 V to -1.09 V vs SCE (became more negative). The increase in the overpotential for zinc deposition was because, with increasing thallium(Ⅰ) ion concentration in the electrolyte, more thallium metal was deposited on the cathode surface and formed microcells with zinc. At the same time, bubbles produced by the hydrogen evolution reaction covered the cathode and thus decreased the effective cathodic area, resulting in a higher current density at the cathode. It resulted in an increase in the cathodic potential for zinc deposition. When the thallium(Ⅰ) ion concentration was less than 0.6 mg L^{-1}, the galvanic cell formed by deposited thallium and zinc had little influence on the zinc electrowinning process. Therefore, as shown in Fig. 1, the current efficiency changed little over this range.

Polarization behaviors

Fig. 6 shows the cathodic polarization curves measured in electrolytes with different thallium(Ⅰ) ion concentrations. When the overpotential was very low, we fitted the linear part of the cathodic polarization curves to obtain the slope, and then calculated the exchange current density according to formula (1). Fig. 7 shows the corrosion potential and corrosion current density of the zinc electrowinning process under different thallium(Ⅰ) ion concentrations using the slope extrapolation method. The above results are shown in Table 1.

$$\eta = -\frac{RTi}{nFi_0} \tag{1}$$

Where η is the overpotential at low overpotential, R is the gas constant, T is the absolute temperature, i is the polarization current density, n is the number of electrons involved in the electrode reaction, F is the Faraday constant, and i_0 is the exchange current density.

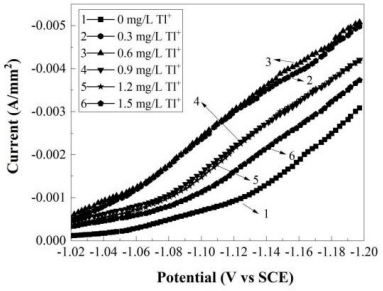

Figure 6. Cathodic polarization curves measured in electrolytes with different thallium(Ⅰ) ion concentrations at a scan rate of 10 mV s^{-1}. Electrolyte: 35.46 g/L Zn^{2+} and 146.05 g/L H_2SO_4 electrolyte with varied Tl(Ⅰ) ions concentration (mg L^{-1}); temperature: 38 ± 1 ℃.

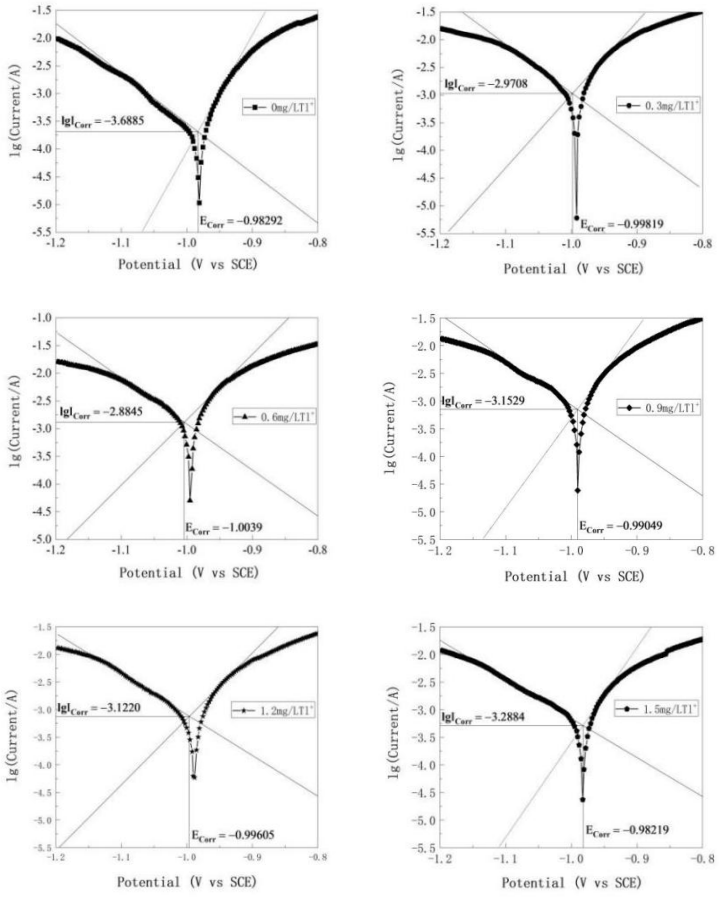

Figure 7. Corrosion potential and corrosion current density obtained by the slope extrapolation method at a scan rate of 10 mV s^{-1}. Electrolyte: 35.46 g/L Zn^{2+} and 146.05 g/L H_2SO_4 electrolyte with varied Tl(Ⅰ) ions concentration (mg L^{-1}); temperature: 38 ± 1 ℃.

Table 1. Corrosion potentials and exchange current densities obtained from cathodic polarization curves, Tafel curves and formula (1).

Tl^+ concentration (mg/L)	0	0.3	0.6	0.9	1.2	1.5
Peak potential (V vs SCE)	-0.98	-0.99	-1.00	-0.99	-0.99	-0.98
Corrosion potential (V vs SCE)	-0.983	-0.998	-1.004	-0.991	-0.996	-0.982
Exchange current density (A/mm^2)	6.9460×10^{-5}	5.6076×10^{-4}	7.5447×10^{-4}	4.0721×10^{-4}	3.1324×10^{-4}	2.4675×10^{-4}

The polarization current density (I_p) in Fig. 6 includes three parts: the first part is the zinc deposition current, the second part is the hydrogen evolution current, and the third part is the current resulting from the galvanic effect. The polarization current density was found to first increase and then decrease with increasing thallium(Ⅰ) ion concentration, with a maximum at the thallium(Ⅰ) ion concentration of 0.6 mg L^{-1}. This indicates that a small amount of thallium(Ⅰ) ions may have a depolarizing effect (promoting hydrogen evolution) during zinc electrowinning. As shown in Table 1, when the concentration of thallium(Ⅰ) ions in the electrolyte was 0.6 mg L^{-1}, the exchange current density of the zinc electrowinning process was maximum and the polarization was minimum. Therefore, when the thallium(Ⅰ) ion concentration increased from 0 mg L^{-1} to 0.6 mg L^{-1}, the hydrogen evolution current increased because a small amount of thallium(Ⅰ) ions may have a depolarization effect during the zinc deposition process. When the thallium(Ⅰ) ion concentration increased from 0.6mg L^{-1} to 1.5mg L^{-1}, with increasing thallium(Ⅰ) ion concentration in the electrolyte, more and more thallium co-deposited with zinc on the cathode, resulting in the galvanic effect. This increased the current produced by the microcells composed of thallium and zinc, decreasing the zinc deposition current and thus the current efficiency. In the microcells, the re-dissolution of zinc would cause thallium to fall off from the cathode surface, so that thallium(Ⅰ) ions would discharge and deposit on the cathode surface again. This cyclic change endangered the zinc electrowinning process. Therefore, when the thallium(Ⅰ) ion concentration was greater than 0.6 mg L^{-1}, a dramatic decrease in current efficiency occurred.

Electrochemical impedance spectroscopy

EIS technique has been employed in electrodeposition of zinc in acidic and alkaline media as well. A correlation between the impedance parameters and film morphology and corrosion resistance has been established in many research papers [24, 25]. After linear polarization experiments, EIS tests were carried out at -1 V, -1.05 V and -1.1 V, respectively, from frequency of 100 kHz to 0.01 Hz, with an amplitude of 10 mV. The Nyquist plots were found to consist of a large capacitive loop at high frequencies, as shown in Figs. 8, 9 and 10.

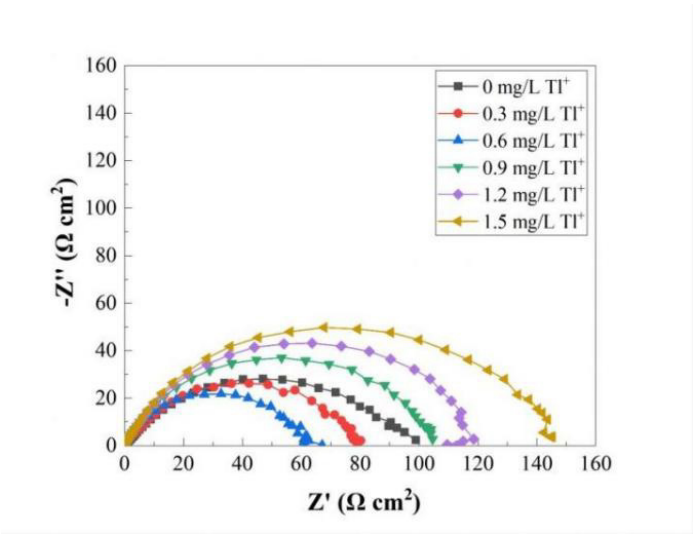

Figure 8. Nyquist plots measured in electrolytes with different thallium(Ⅰ) ion concentrations at a voltage of -1 V. Electrolyte: 35.46 g/L Zn^{2+} and 146.05 g/L H_2SO_4 electrolyte with varied Tl(Ⅰ) ion concentration; temperature: 38 ± 1 ℃.

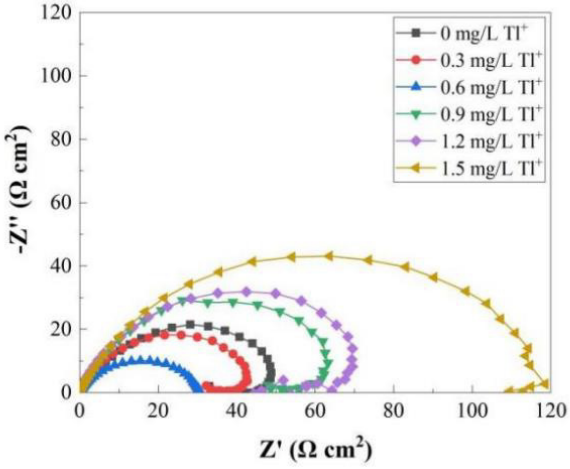

Figure 9. Nyquist plots measured in electrolytes with different thallium(Ⅰ) ion concentrations at a voltage of -1.05 V. Electrolyte: 35.46 g/L Zn^{2+} and 146.05 g/L H_2SO_4 electrolyte with varied Tl(Ⅰ) ion concentration; temperature: 38 ± 1 ℃.

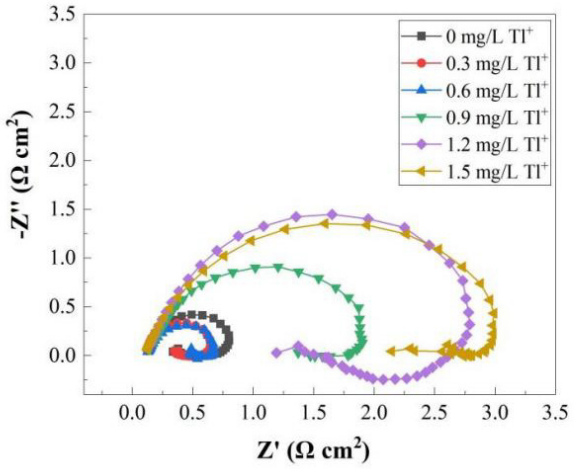

Figure 10. Nyquist plots measured in electrolytes with different thallium(Ⅰ) ion concentrations at a voltage of -1.1 V. Electrolyte: 35.46 g/L Zn^{2+} and 146.05 g/L H_2SO_4 electrolyte with varied Tl(Ⅰ) ion concentration; temperature: 38 ± 1 ℃.

The high frequency capacitive loop is usually attributed to the charge transfer resistance across the double layer. The electrochemical impedance data measured at a voltage of -1 V (Fig. 8) were modelled using the equivalent circuit presented in Fig. 11. This model consists of a solution resistance term (R_s), charge transfer resistance (R_{ct}) in the electrode reaction, and a constant phase element (CPE), which was used to model a double layer capacitance of the electrode/electrolyte interface. The impedance of CPE is defined by two parameters: CPE-T and CPE-P. Generally, when there is a dispersion effect on the electrode surface, the CPE-P value is always between 0.5 and 1. The corrosion current density is usually a parameter that characterizes the degree of corrosion of an electrode or material in an electrochemical environment. During the electrodeposition process, the corrosion of the electrode surface may occur simultaneously with the electrodeposition reaction. Appropriate corrosion current density can adjust the current efficiency to a certain extent. By understanding the relationship between the corrosion current density and the electrolysis conditions, the electrolyte composition, current density, temperature, and other parameters were adjusted to maximize the electrowinning efficiency and product quality. The corrosion current was calculated using impedance parameters employing the following equation (formula (2)):

$$i_{corr} = \frac{b_a \times b_c}{b_a + b_c} \times \frac{1}{R_{ct}} \quad (2)$$

where, b_a and b_c are the slopes of the anode and cathode Tafel, respectively. R_{ct} is the charge transfer resistance obtained from the EIS measurements.

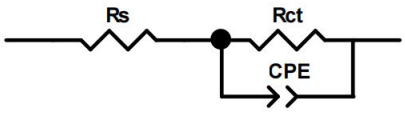

Figure 11. Equivalent circuit used to model the EIS data at a voltage of -1 V.

The degree of fitting between the measured EIS data and calculated results is evaluated by minimizing the chi-square statistic (χ^2). It is generally believed that it is acceptable when the chi-square value is less than or equal to 10^{-3} (order of magnitude). All measured impedance parameters were listed in Table 2. The chi-square values between calculated results and measured data were within 10^{-4} (order of magnitude), which depicted the best fitting agreement of the equivalent circuit model. The results revealed that, When the thallium(Ⅰ) ion concentration increased from 0 mg L^{-1} to 0.6 mg L^{-1}, the R_{ct} decreased from 97.94 Ω cm^2 to 60.19 Ω cm^2; when the thallium(Ⅰ) ion concentration increased from 0.6 mg L^{-1} to 1.5 mg L^{-1}, the R_{ct} increased from 60.19 Ω cm^2 to 142.27 Ω cm^2, indicating that a small amount of thallium(Ⅰ) ions accelerated the electrode reaction which reached the fastest at 0.6 mg L^{-1}. CPE is commonly used to describe the behavior of non-ideal double-layer capacitance. This non-ideal pure capacitance characteristic of CPE is usually caused by electrode surface non-uniformity, roughness, electrode porosity, and the uneven distribution of current and potential related to electrode geometry. When the thallium(Ⅰ) ion concentration was 0.6 mg L^{-1}, the CPE value was minimum, the charge transfer rate was maximum, and the electrode reaction was fastest, showing the maximum corrosion current density.

Table 2. Electrochemical parameters of the zinc sulfate system with different thallium(Ⅰ) ion concentrations at a voltage of -1 V fitted by EIS and corrosion current densities calculated by formula (2).

Tl^+ conc (mg/L)	R_s (Ω cm^2)	R_{ct} (Ω cm^2)	CPE (F cm^{-2})	CPE-P (n)	Chi-Squared (χ^2)	I_{corr} (A/mm^2)
0	0.07636	97.94	8.771×10^{-4}	0.678	5.829×10^{-4}	0.001782
0.3	0.06245	79.66	4.121×10^{-4}	0.724	6.590×10^{-4}	0.001975
0.6	0.08123	60.19	2.990×10^{-4}	0.837	9.270×10^{-4}	0.002773
0.9	0.07925	102.18	3.312×10^{-4}	0.810	9.349×10^{-4}	0.001806
1.2	0.08136	116.15	3.414×10^{-4}	0.807	9.493×10^{-4}	0.001722
1.5	0.08101	142.27	3.621×10^{-4}	0.797	7.184×10^{-4}	0.000928

In Fig. 9 and even more prominently in Fig. 10, a low-frequency inductive loop was present. Therefore, the electrochemical impedance data measured at a voltage of -1.1 V (Fig. 10) were modelled using the equivalent circuit presented in Fig. 12. In the low-frequency region, the induction loop was related to the adsorption of intermediate products on the electrode surface, represented by a resistance (R_L) and inductance (L_1). All measured impedance parameters were listed in Table 3. When the intermediate product appeared in the electrode reaction, the intermediate product adsorbed and produced a surface adsorption complex on the surface of the metal electrode. The surface complex was produced in the first step of the electrode reaction and consumed in the second step. Therefore, an inductive arc appeared in the low-frequency part of the impedance diagram. The deposition of zinc in zinc electrowinning was mainly carried out in two steps. First, Zn^{2+} obtained an electron to form an adsorbed zinc monovalent ion, and then another electron was obtained to form an active zinc molecule. From Table 3, it can be seen that at -1.1 V potential, with the increase in Tl^+ concentration, the R_{ct} of zinc electrowinning decreased first and then increased, and the CPE-P was all less than 1, indicating that the electrode surface was relatively rough. When the concentration of Tl^+ was 0.6 mg L^{-1}, the R_{ct} and CPE of zinc electrowinning were minimum. When the concentration of Tl^+ increased from 0 mg L^{-1} to 0.6 mg L^{-1}, the adsorption resistance R_L did not change much, and the inductance L_1 caused by the surface diffusion of adsorbed atoms decreased. When the concentration of Tl^+ increased from 0.6 mg L^{-1} to 1.5 mg L^{-1}, the adsorption resistance R_L and the inductance L_1 caused by surface diffusion of adsorbed atoms increased significantly. This may be because the zinc monovalent ions generated in the first step of zinc electrowinning were adsorbed on the electrode surface. As the concentration of Tl^+ increased to 1.5 mg L^{-1}, the adsorption of zinc monovalent ions was more difficult and the adsorption behavior was more complex, resulting in an increase in R_{ct}, R_L and L_1.

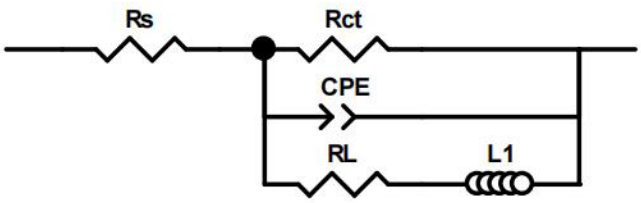

Figure 12. Equivalent circuit used to model the EIS data at a voltage of -1.1 V.

Table 3. Electrochemical parameters of the zinc sulfate system with different thallium(Ⅰ) ion concentrations at a voltage of -1.1 V fitted by EIS.

Tl^+ conc (mg/L)	R_s (Ω cm^2)	R_{ct} (Ω cm^2)	CPE (F cm^{-2})	CPE-P (n)	R_L (Ω cm^2)	L_1 (H cm^2)	Chi-Squared (χ^2)
0	0.1197	1.4262	3.841×10^{-3}	0.899	0.7370	1.90×10^{-3}	4.328×10^{-4}
0.3	0.1086	1.0246	4.818×10^{-3}	0.898	0.7084	1.92×10^{-3}	7.569×10^{-4}
0.6	0.0996	0.8280	5.796×10^{-4}	0.923	0.8051	8.00×10^{-4}	8.964×10^{-4}
0.9	0.1053	3.2713	6.787×10^{-4}	0.706	2.9346	8.64×10^{-4}	9.584×10^{-4}
1.2	0.1082	4.2789	6.019×10^{-3}	0.828	3.6273	9.46×10^{-2}	9.527×10^{-4}
1.5	0.1103	4.3429	6.248×10^{-3}	0.845	3.6857	9.34×10^{-2}	8.193×10^{-4}

CONCLUSIONS

Concerning the effect of thallium(Ⅰ) ions on the electrowinning of zinc from acidic sulfuric acid electrolytes, the following conclusions were obtained:

(1) With increasing thallium(Ⅰ) ion concentration in the electrolyte, the hydrogen evolution reaction and the galvanic effect produced during zinc electrowinning increased. This led to the re-dissolution of cathode zinc, which influenced the morphology of the obtained zinc deposits and severely reduced the current efficiency.

(2) A small amount of thallium(Ⅰ) ions in the electrolyte had a depolarization effect during zinc deposition, which increased the hydrogen evolution current. When the concentration of thallium(Ⅰ) ions in the electrolyte was 0.6 mg L^{-1}, the exchange current density of the zinc electrowinning process was maximum and the polarization was minimum. When the thallium(Ⅰ) ion concentration increased from 0.6 mg L^{-1} to 1.5 mg L^{-1}, with increasing thallium(Ⅰ) ion concentration in the electrolyte, more and more thallium co-deposited with zinc on the cathode, resulting in the galvanic effect.

(3) When the concentration of thallium(Ⅰ) ions was 0.6 mg L^{-1}, the R_{ct} of the equivalent circuit was minimum, the CPE value was minimum, the charge transfer rate was maximum, and the electrode reaction was fastest, showing the maximum corrosion current density. When EIS tests were carried out at -1.1 V, a low-frequency inductive loop was present. At this time, when the concentration of Tl^+ increased from 0 mg L^{-1} to 0.6 mg L^{-1}, the adsorption resistance R_L did not change much, and the inductance L_1 caused by the surface diffusion of adsorbed atoms decreased. When the concentration of Tl^+ increased from 0.6 mg L^{-1} to 1.5 mg L^{-1}, the adsorption resistance R_L and the inductance L_1 caused by surface diffusion of adsorbed atoms increased significantly.

EXPERIMENTAL SECTION

The electrolyte used in this study was prepared with distilled water, 0.1 g/L terpenic oil, 35.46 g/L Zn^{2+}, and 146.05 g/L H_2SO_4 as the base electrolyte for different concentrations of thallium(Ⅰ) ions. All electrochemical measurements were carried out using the Autolab PGSTAT 302N electrochemical workstation. The three-electrode system was used in the experiment. The saturated calomel electrode was used as the reference electrode. The auxiliary electrode was a square platinum electrode of 1 cm × 1 cm. The working electrode was a circular glassy carbon electrode with a diameter of 2 mm. The working electrode was polished, then soaked in alcohol for 5 minutes, and finally cleaned with distilled water before use. This cathode pretreatment procedure was essential to obtaining reproducible results. A Luggin capillary was used to reduce the ohmic drop from the solution. In all electrochemical measurements, the anode to cathode surface area ratio was greater than 50. This ensured that the anodic process had a negligible influence on the cathodic process because the anodic current density of polarization and anodic polarization potential were less than the cathodic current density and polarization potential. The cathodic polarization curves were measured at a scan rate of 10 mV s^{-1}.

During all the electrodeposition experiments, the cathode current density was maintained at 518.86 A m^{-2}, and the electrolysis time was 24 h. The temperature of the electrolytic cell was maintained at 38 ± 1 ℃ in a constant temperature bath. The current efficiency (η) was obtained from the following equation:

$$\eta = \frac{2mF}{MIt} \times 100\% \quad (3)$$

where m is the mass of Zn deposited on the cathode, M is the molar mass of zinc (M = 65.39 g mol^{-1}), I is the cathodic current, t is the electrowinning time, and F is the Faraday constant (F = 96485 C mol^{-1}).

The deposited morphology was examined by a scanning electron microscope (SEM).

ACKNOWLEDGMENTS

The authors acknowledge the funding support from the Applied Basic Research Project of Yunnan (No. 202001BA070001-135) and the Scientific Research Foundation of Education Department of Yunnan Province of China (No. 2022Y751).

REFERENCES

1. F. Porter; *Zinc Handbook,* Faulkener, New York, **1991**, ISBN: 9780824783402.
2. S. Gürmen; M. Emre; *Miner. Eng.,* **2003**, *16,* 559-562.
3. A. E. Saba; A. E. Elsherief; *Hydrometallurgy,* **2000**, *54,* 91-106.
4. H. Zhang; Y. Li; J. Wang; X. Hong; *Hydrometallurgy,* **2009**, *99,* 127-130.
5. F. Parada T; E. Asselin; *JOM,* **2009**, *61,* 54-58.
6. I. Ivan; St. Rashkov; *Stud. Univ. Babes-Bolyai Chem.,* **1996**, *2,* 122-137.
7. L. Muresan; G. Maurin; L. Oniciu; *Hydrometallurgy,* **1996**, *43,* 345-354.
8. J. Q. Zhu; Y. M. Wu; J. Zuo; D. F. Khan; C. H. Jiang; *Hydrometallurgy,* **2017**, *174,* 248-252.
9. M. Saloma; H. Holtan Jr; *Acta Chem. Scand.,* **1974**, *28a,* 86-92.
10. J. Wu; P. Zeng; Q. Feng; Z. M. Liu; W. J. Qiu; S. B. Zhang; Q. S. Yang; Y. Jiang; *China Nonferrous Metallurgy,* **2021**, *50,* 34-38 (in Chinese).
11. J. Liu; J. Wang; Y. H. Chen; X. F. Xie; J. Y. Qi; H. Lippold; D. G. Luo; C. L. Wang; L. X. Su; L. C. He; Q. W. Wu; *Environ. Pollut.*, **2016**, *212*, 77-89.
12. B. Karbowska; W. Zembrzuski; M. Jakubowska; T. Wojtkowiak; A. Pasieczna; Z. Lukaszewski; *J. Geochem. Explor.*, **2014**, *143*, 127-135.
13. Y. Liu; W. P. Chen; Y. H. Huang; Z. H. Li; C. S. Li; H. X. Liu; X. L. Huangfu; *J. Hazard. Mater.*, **2024**, *462*, 132745.
14. F. G. Zhao; *Non-Ferrous Mining and Metallurgy,* **2008**, *24,* 24-26 (in Chinese).
15. A. M. Abd El-Halim; R. M. Khalil; *Surf. Technol.*, **1984**, *23*, 215-223.
16. J. Clavilier; J. P. Ganon; M. Petit; *J. Electroanal. Chem.,* **1989**, *265,* 231-245.
17. P. Rodriguez; N. García-Aráez; E. Herrero; J. M. Feliu; *Electrochim. Acta,* **2015**, *151,* 319-325.
18. M. Hosseini; S. Ebrahimi; *J. Electroanal Chem.,* **2010**, *645,* 109-114.
19. H. J. Wang; X. Wang; Z. Jin; *China Nonferrous Metallurgy,* **2022**, *51,* 105-111 (in Chinese).
20. Y. J. Zou; H. J. Cheng; H. N. Wang; R. X. Huang; Y. H. Xu; J. Jiang; Q. He; C. H. Liu; J. C. Liu; J. M. Xiong; J. N. Yao; X. L. Huangfu; J. Ma; *Environ. Sci. Technol.,* **2020**, *54,* 7205-7216.
21. Z. M. Senol; U. Ulusoy; *Chem. Eng. J.,* **2010**, *162,* 97-105.
22. B.G. Xiong; S. F. Liu; Y. Wang; Z. M. Xia; L. G. Ye; *J. Clean. Prod.*, **2023**, *430*, 139695.
23. T. J. Yang; J. H. Kong; J. Tao; B. Xu; G. F. Dong; H. F. Shang; *China Nonferrous Metallurgy,* **2019**, *48,* 29-32 (in Chinese).
24. D. Desai; X. Wei; D. A. Steingart; S. Banerjee; *J. Power Sources,* **2014**, *256,* 145-152.
25. X. Wei; D. Desai; G. G. Yadav; D. E. Turney; A. Couzis; S. Banerjee; *Electrochim. Acta,* **2016**, *212,* 603-613.